

A Model of Short Gamma-Ray Bursts: Heated Neutron Stars in Close Binary Systems

Jay D. Salmonson

James R. Wilson

Lawrence Livermore National Laboratory, P.O. Box 808, Livermore, CA 94550

ABSTRACT

In this paper we present a model for the short (< 1 second) population of gamma-ray bursts. In this model heated neutron stars in a close binary system near its last stable orbit emit a large amount of neutrinos ($\sim 10^{53}$ ergs). A fraction of these neutrinos will annihilate to form an e^+e^- pair plasma wind which will, in turn, expand and recombine to photons which make the gamma-ray burst. We study neutrino annihilation and show that a substantial fraction ($\sim 1/2$) of energy deposited into e^+e^- pairs comes from inter-star neutrinos, where each member of the neutrino pair originates from each neutron star. Thus, in addition to the annihilation of neutrinos blowing off of a single star, there is a new source of baryon-free plasma that is deposited between the stars. To model the e^+e^- pair plasma wind between stars, we do three-dimensional relativistic numerical hydrodynamic calculations. We find that the time scale for these bursts, deriving from the baryon-free plasma, is less than one second and they will have a hot spectrum ~ 5 MeV. The energy in bursts is the order of 10^{52} ergs.

Subject headings: gamma rays: bursts — gamma rays: theory

1. Introduction

In Salmonson et al. (2001) we investigated a model for gamma-ray bursts (GRBs) deriving from a neutrino burst of energy $\sim 10^{53}$ ergs above a heated, collapsing neutron star in a binary. Such conditions have been suggested by numerical relativistic hydrodynamic simulations (Mathews & Wilson 2000) of compression, heating and collapse of binary neutron stars near their last stable orbit. Such a thermal neutrino burst was found to partially recombine via $\nu\bar{\nu} \rightarrow e^+e^-$ into an e^+e^- pair plasma which expands relativistically. This fireball then recombines into photons via $e^+e^- \rightarrow \gamma\gamma$ and was found to give a gamma-ray burst of energy $\sim 10^{51} - 10^{52}$ ergs with spectral and temporal characteristics consistent with observations.

This paper elaborates on the previous work in three distinct ways. 1) The latest general relativistic hydrodynamic calculations by Wilson and Mathews indicate that evolution and compression of the stars in a binary is faster than previously thought; $\lesssim 1$ sec, thus making this process a more natural candidate for the generation of “short” GRBs ($\lesssim 1$ sec). 2) Herein we use recent work by Salmonson & Wilson (2001) which calculates the neutrino annihilation rate *between* two neutron stars in addition to the annihilation rate from a single star (Salmonson & Wilson 1999). This ‘inter-star’ annihilation will not drive a baryon wind from the stellar surface and thus we find no baryon loading in the e^+e^- pair plasma that originates between the neutron stars. 3) We employ three dimensional (3D) relativistic hydrodynamic calculations to model the flow of the wind in the complex, rotating, strong gravity environment around the neutron stars.

It has been known for some time that the population of GRBs is bimodal, with approximately a third of bursts having durations less than 2 seconds, and these short bursts typically have harder spectra than those bursts lasting longer than 2 seconds (Kouveliotou et al. 1993). This bimodality is thought to indicate that short and long bursts are separate populations and mechanisms. This view is bolstered by evidence that spectral break energy (Paciesas et al. 2001) and pulse lags (Norris et al. 2000) have a discontinuous jump between short and long populations. The lack of discovery and location of an afterglow associated with short bursts has severely impeded progress in determining the distance scale and thus the energetics of these bursts. In fact, comparisons of BeppoSAX and BATSE data archives indicates a dearth of X-ray afterglows (Gandolfi 2001). Analysis of BATSE data for short burst decay tails give conflicting results indicating both a lack of an underlying afterglow component (Connaughton 2000) and the existence of such a component (Lazzati et al. 2001).

2. The Model

In this model we estimate that 10% of the rotationally enhanced binding energy of a neutron star ($\sim 10^{53}$ ergs) is converted to thermal energy via compression, vortices and shocks. This 10^{53} ergs of energy is released as a monotonically increasing luminosity of neutrinos over a timescale of order $\sim 1/10$ second as estimated by Mathews & Wilson (1997). This neutrino luminosity $\sim 10^{54}$ ergs s^{-1} annihilates into an e^+e^- pair plasma. Annihilation of high neutrino luminosities in the strong gravitational field of the neutron stars can have high efficiencies; near unity (Salmonson et al. 2001). About half of the pair plasma energy is deposited uniformly around the neutron stars due to single star neutrino annihilation (Salmonson & Wilson 1999) and the other half is deposited between the stars due to interstar neutrino annihilation (Salmonson & Wilson 2001).

This plasma deposition morphology then becomes input for the 3D relativistic hydrodynamic code, which calculates the expansion of the plasma (Figure 1). These simulations show a plasma of very high entropy expanding out along the plane of symmetry between the neutron stars. In the regions around the stars lower entropy plasma is formed because a baryon wind is blown from the stars. The numerical model follows the baryons, hence some baryons were added in the interstellar region. The calculation yields an estimate of the angular distribution of the baryonic loading of the plasma.

Thus this model predicts a variety of bursts. Viewed along the axis of rotation, a prompt quasi-thermal burst of duration $\sim 1/10$ second will result from the annihilation of fireball pairs (Salmonson et al. 2001). Because of the dearth of baryons left over to sweep into the interstellar medium, we do not predict the existence of an afterglow. This agrees with preliminary searches of the data archives for short-burst afterglows, which appear to be missing (Gandolfi 2001).

Viewed far from the axis of rotation a very different burst results. The lower entropy means that there will not be a prompt burst from pair annihilation in the fireball. However, there will be a baryon wind sweeping into the interstellar medium. Thus we expect a burst that decays into an afterglow as a power-law (Salmonson et al. 2001). This behavior will be made chaotic and complex by the rapid rotation of the binary system.

3. One-Dimensional Calculations

Using one-dimensional (1D) relativistic hydrodynamics described in Salmonson et al. (2001), we can study the expansion of an e^+e^- pair plasma fireball from the surface of a single neutron star. As per our model, we deposit $\mathcal{E} = 10^{52}$ ergs of energy into a narrow (width = 1 km) shell region above the surface of a $R_0 = 10$ km radius and $1.4 M_\odot$ mass neutron star. We monotonically ramp the energy over $\Delta t = 0.1$ second. This model is run with a range of deposited baryon densities and thus a range of baryon loadings of the fireball.

It is important to note that our hydrodynamics do not track the protons and neutrons separately and, as such, assumes they are well coupled during the expansion and acceleration of the plasma. As was shown by Fuller et al. (2000) and Derishev et al. (1999), the neutrons can decouple from the protons and e^+e^- plasma during acceleration, thus changing the overall baryon load of the plasma. Since it is plausible that the baryon matter blown off of the neutron star is 90% neutrons, it is reasonable to expect, depending on the efficiency of the decoupling, the effective baryon mass to be a factor of several less than the total baryon mass.

The plasma fireball is evolved and we find that it expands adiabatically as a thin shell of constant coordinate thickness ΔR (Ruffini et al. 2000). We track this expansion and pair annihilation until the optical depth, τ , of the plasma falls below unity: $\tau \sim N\sigma_T\Delta R < 1$ where N is the coordinate density of electrons and positrons and σ_T is the Thompson cross-section. The energy in photons, E_{photons} , and in the baryons, E_{baryons} , is calculated and these results are summarized in Fig. (2). One can see that for $\mathcal{E}/\mathcal{M} \lesssim 10^5$, where \mathcal{M} is the baryonic rest mass energy, most of the energy goes into accelerating the baryons while for $\mathcal{E}/\mathcal{M} \gtrsim 10^5$ a substantial fraction of the energy is expressed as photons directly from the plasma; i.e. a gamma-ray burst.

This result can be understood when one considers that the opacity of the fireball derives from two electron densities: electrons associated with entrained protons, $N_{\text{electrons}} = N_{\text{protons}}$, and electrons and positrons in pairs, N_{pairs} . Defining the optical depth as $\tau = \tau_{\text{electrons}} + \tau_{\text{pairs}} \approx (N_{\text{protons}} + N_{\text{pairs}})\sigma_T\Delta R$, then by comparing the densities N_{protons} and N_{pairs} , we understand the relative importance of these two sources of opacity.

We first consider the baryons. Equating the energy deposition with outgoing flux gives the initial energy density at the surface of the neutron star $E_0 = \mathcal{E}/(\Delta t 4\pi R_0^2 c) \approx 3 \times 10^{29}$ ergs cm^{-3} . It follows that the corresponding initial number density of baryons is $N_{b,0} = E_0/m_p c^2 (\mathcal{M}/\mathcal{E}) \approx 1.3 \times 10^{35} (\mathcal{M}/\mathcal{E}) \text{cm}^{-3}$, where \mathcal{M}/\mathcal{E} is the ratio of baryon rest mass energy to total energy. Finally, we know (Ruffini et al. 2000) that for relativistic adiabatic expansion we have: $N_b = N_{b,0} (R_0/R)^2$. Let us assume that 10% of the baryons are protons with associated electrons. Then the optical depth from the entrained baryons is $\tau_{\text{electrons}} \approx 0.1 N_b \sigma_T \Delta R \sim 0.1 (E_0/m_p c^2) (\mathcal{M}/\mathcal{E}) (R_0/R)^2 \sigma_T \Delta R$ and thus optical thinness, $\tau_{\text{electrons}} \approx 1$ happens at a radius $R_{\text{baryons}} \sim 10^{12} \sqrt{(\mathcal{M}/\mathcal{E})_{-5}}$ cm, where $(\mathcal{M}/\mathcal{E})_{-5} \equiv (\mathcal{M}/\mathcal{E})/10^{-5}$. Notice that this radius depends on the initial baryon loading of the fireball: $R_{\text{baryons}} \propto \sqrt{\mathcal{M}/\mathcal{E}}$.

The opacity due to pairs is a bit more complex. As discussed in Salmonson et al. (2001), the pair number density is governed by the following equation

$$\frac{\partial N_{\text{pairs}}}{\partial t} = -\frac{\alpha}{r^2} \frac{\partial}{\partial r} \left(\frac{r^2}{\alpha} N_{\text{pairs}} V^r \right) + \overline{\sigma_{\text{ann}} v} ((N_{\text{pairs}}^0(T'))^2 - N_{\text{pairs}}^2) / W^2 \quad (1)$$

where $\overline{\sigma_{\text{ann}} v}$ is the Maxwellian averaged mean pair annihilation rate per particle and $N_{\text{pairs}}(T')$ is the local coordinate equilibrium e^+e^- pair density at local temperature T' given by the appropriate Fermi integral with a chemical potential of zero. Early in the fireball expansion e^+e^- pairs are in equilibrium so $N_{\text{pairs}} \approx N_{\text{pairs}}^0(T')$ and thus the pairs expand adiabatically: $N_{\text{pairs}} = N_{\text{pairs},0} (R_0/R)^2$, where the initial pair number density is given by $N_{\text{pairs},0} \sim (aE_0^3)^{1/4}/3k \sim 10^{34} \text{cm}^{-3}$. When the local temperature, T' , of the plasma falls below $T'_* \simeq m_e c^2/3 \sim 1/6$ MeV the pairs begin to rapidly annihilate. This happens at a radius $R_* \sim R_0/T'(E_0/a)^{1/4} \sim 100R_0$. The pair number density plummets

until the annihilation term in Eqn. (1) no longer dominates, which happens at a density $N_{pair,*} \sim R_*/(\overline{\sigma_{ann}}R_0^2) \sim 10^{20}\text{cm}^{-3}$. This annihilation happens over a few R_* which is very small compared to the radius at which pairs and photons decouple and therefore these results are independent of the details of this annihilation phase. Beyond this point the pair number density again expands adiabatically: $N_{pair} = N_{pair,*}(R_*/R)^2$. Thus the optical depth from the pairs is $\tau_{pairs} \approx N_{pairs}\sigma_T\Delta R \sim (E_0/a)^{1/4}\sigma_T\Delta R/(\overline{\sigma_{ann}}R_0T_*'^3)(R_0/R)^2$ and optical thinness, $\tau_{pairs} \approx 1$, happens at a radius $R_{pairs} \sim \sqrt{(E_0/a/T_*')^{3/4}\sigma_TR_0\Delta R/\overline{\sigma_{ann}}} \sim 10^{12}$ cm which is independent of \mathcal{E}/\mathcal{M} .

Thus we see that the transition shown in Fig. (2) from baryon-dominated to photon-dominated fireball energy is governed by the relative importance of opacity associated with the baryons and that associated with the e^+e^- pairs. Therefore it is important to consider both the opacity due to electrons associated with protons, which dominate for high baryon loading, and the opacity of the e^+e^- pair plasma which dominates for low baryon loads. For initial values $\mathcal{E}/\mathcal{M} < 10^5$, $R_{\text{baryons}} > R_{\text{pairs}}$ so the opacity is dominated by the electrons associated with the baryons and thus the baryons are able to “hold” the plasma longer and thus absorb all of the fireball energy. For $\mathcal{E}/\mathcal{M} > 10^5$ we have $R_{\text{pairs}} > R_{\text{baryons}}$ and the pairs are the dominant source of opacity and thus determine the radius of optical thinness. If the radius of optical thinness falls below the radius to saturate the energy of the baryons, i.e. the radius at which most of the plasma energy is in the baryons, $R_{\text{saturnate}} = (\mathcal{E}/\mathcal{M})R_0$, then the acceleration of the baryons is inefficient, they do not attain the energy $(\mathcal{E}/\mathcal{M})m_p c^2$, and thus more energy remains in the photons, thus yielding a photon burst.

4. Three-Dimensional Calculations

While the 1D hydrodynamics of the last section elucidate the behavior of an expanding relativistic plasma, a 3D calculation is required to capture the structure inherent in the present problem of rotating, emitting binary neutron stars. In this section we introduce the 3D relativistic hydrodynamic equations. Herein we use units $G = c = 1$. The continuity equation is

$$\frac{\partial D}{\partial t} = -6D \frac{\partial \log \phi}{\partial t} - \frac{1}{\phi^6} \frac{\partial(\phi^6 DV^i)}{\partial x^i}. \quad (2)$$

where the spatial dimensions are indicated by the sum over $i = 1, 2, 3$. The energy equation is

$$\frac{\partial E}{\partial t} = -6\Gamma E \frac{\partial \log \phi}{\partial t} - \frac{1}{\phi^6} \frac{\partial(\phi^6 EV^i)}{\partial x^i} - P \left[\frac{\partial W}{\partial t} + \frac{1}{\phi^6} \frac{\partial(WV^i \phi^6)}{\partial x^i} \right]. \quad (3)$$

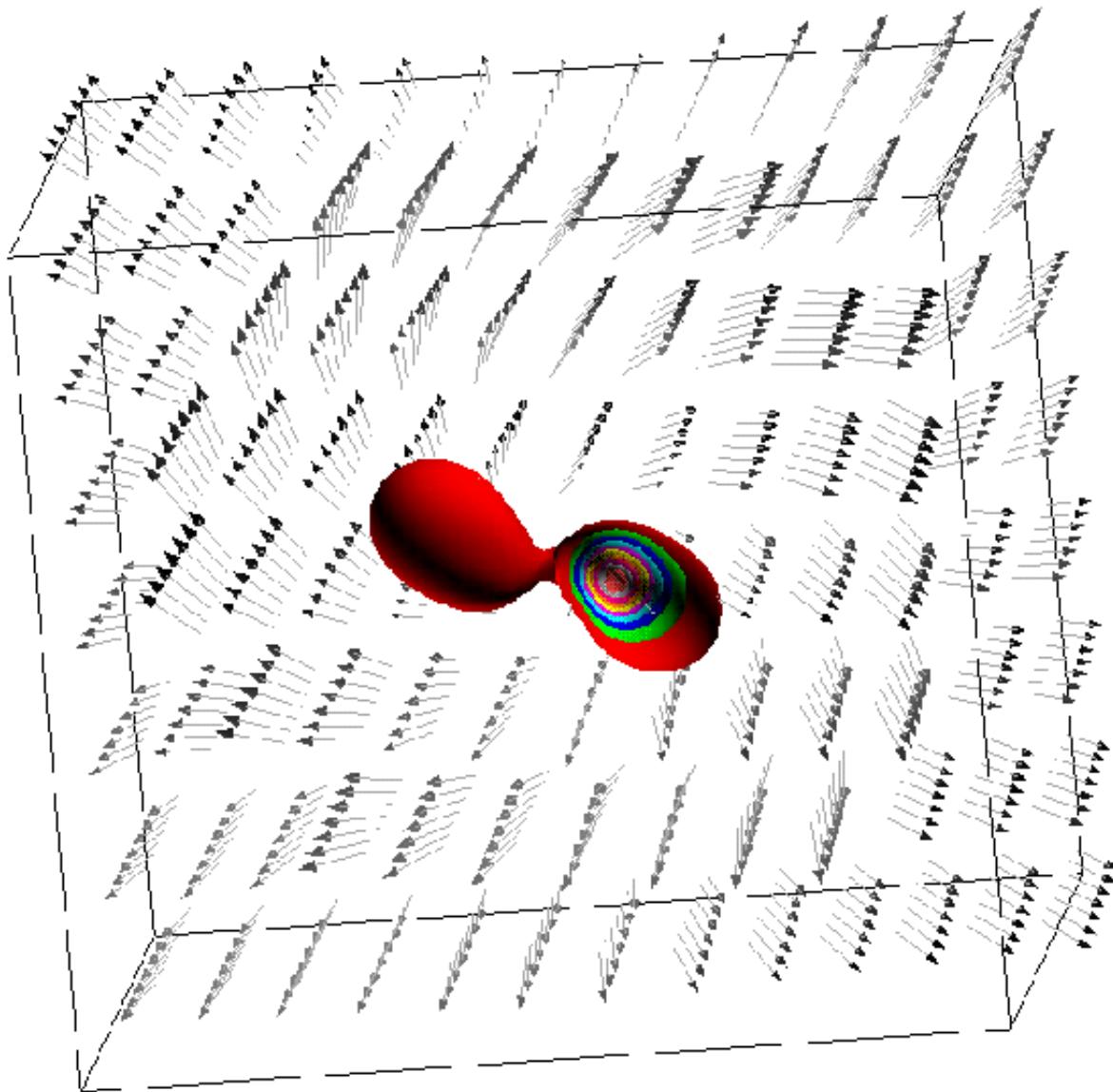


Fig. 1.— Three dimensional relativistic simulation of two 10 km radius neutron star separated by 30 km emitting 10^{53} ergs/sec of energy in e^+e^- pair plasma and about 1 % equivalent mass in baryons. The contour map, with right star cutaway, is of baryon density. The vector field is the 3-velocity of expanding plasma. This problem settles down to a static flow after about one orbit with period $\sim 1/300$ second.

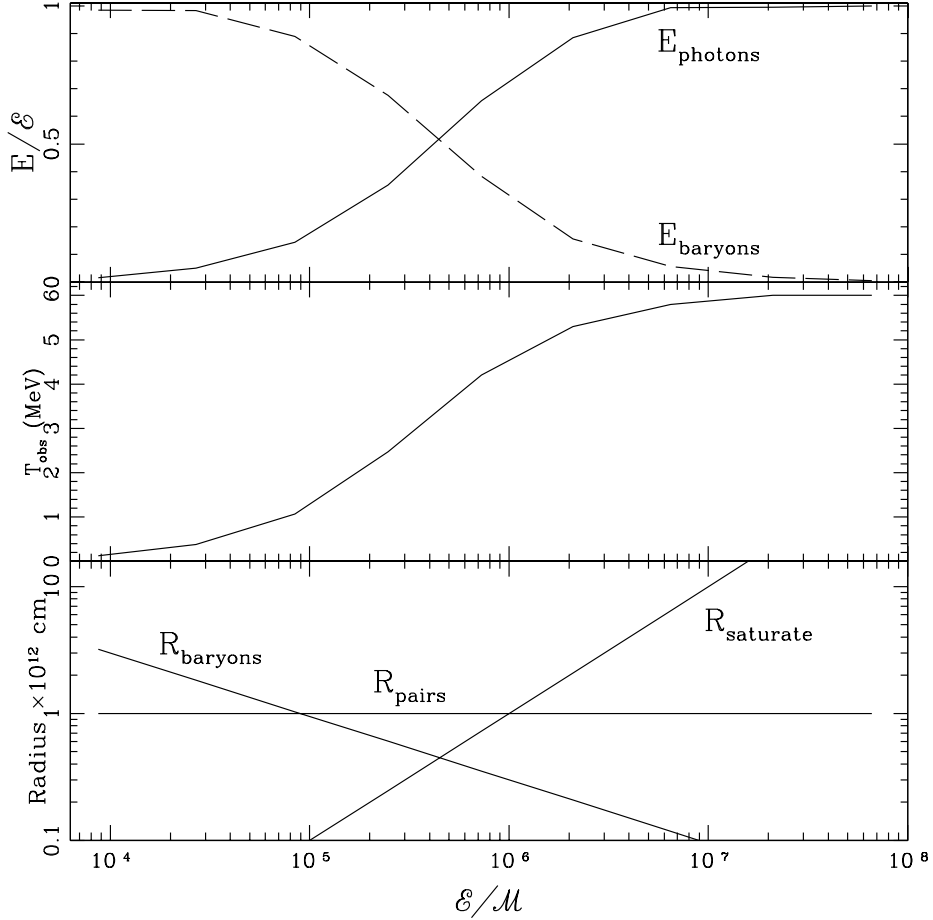


Fig. 2.— Output of the 1D code run over a range of initial energy-to-mass ratios, \mathcal{E}/\mathcal{M} , with energy fixed at $\mathcal{E} = 10^{52}$ ergs. This shows that the energy available for creation of an internal burst versus that for an external burst varies as a function of baryon loading. The more baryon loading (lower \mathcal{E}/\mathcal{M}), the more energy is entrained in the baryons, E_{baryons} , and thus creates a more energetic external shock. Less baryon loading (higher \mathcal{E}/\mathcal{M}) makes a more efficient fireball burst, where much of the original energy is left in the photons, E_{photons} . The middle figure shows the typical observed temperature, T_{obs} , of the resultant photons. The lower figure shows the characteristic radii determining the evolution: $R_{\text{baryons}} \approx 10^{12} \sqrt{(\mathcal{M}/\mathcal{E})_{-5}}$ cm, $R_{\text{pairs}} \approx 10^{12}$ cm, $R_{\text{saturnate}} \approx 10^6 (\mathcal{E}/\mathcal{M})$ cm. The photons decouple from the baryons at the maximum, R_{baryons} or R_{pairs} . If $R_{\text{saturnate}}$ is greater than either R_{baryons} or R_{pairs} , then the baryons are unable to saturate with energy and thus the energy remains in the photons.

And the momentum equations are

$$\begin{aligned} \frac{\partial S_i}{\partial t} = & -6S_i \frac{\partial \log \phi}{\partial t} - \frac{1}{\phi^6} \frac{\partial(\phi^6 S_i V^j)}{\partial x^j} - \alpha \frac{\partial P}{\partial x^i} - W(D + \Gamma E) \frac{\partial \alpha}{\partial x^i} \\ & + S_j \frac{\partial \beta^j}{\partial x^i} + 2\alpha(D + \Gamma E) \left[W - \frac{1}{W} \right] \frac{\partial(\log \phi)}{\partial x^i}, \end{aligned} \quad (4)$$

where the four-velocity is

$$U_i = \frac{S_i}{D + \Gamma E}, \quad (5)$$

and we define a generalized Lorentz factor

$$W = \sqrt{1 + \frac{\Sigma(U_i)^2}{\phi^4}}, \quad (6)$$

the coordinate velocity in terms of the four velocity (eqn. 5) is given by

$$V^i = \frac{\alpha U_i}{W \phi^4} - \beta^i, \quad (7)$$

and the equation of state is given by

$$\Gamma = 1 + \frac{PW}{E}. \quad (8)$$

The metric is 3+1 and taken to be conformally flat. The lapse function is given by

$$\alpha \equiv \left(\frac{1 - \frac{F}{2}}{1 + \frac{F}{2}} \right). \quad (9)$$

The spatial factor is

$$\phi \equiv 1 + \frac{F}{2}, \quad (10)$$

and the shift vector is

$$\beta^\phi \propto \Omega \times \mathbf{r} - A \left(\frac{M_1}{r_1} - \frac{M_2}{r_2} \right). \quad (11)$$

The factor F is defined by

$$F \equiv \begin{cases} \frac{M}{r_1} + \frac{M}{r_2} & r_1 > R_\star \\ \frac{M}{2} \left(\frac{3}{R_\star} - \frac{r_1^2}{R_\star^3} \right) + \frac{M}{r_2} & r_1 < R_\star \end{cases} \quad (12)$$

where r_1 and r_2 are the distances from the center of the nearest and farthest stars respectively, each of mass M and radius R_\star .

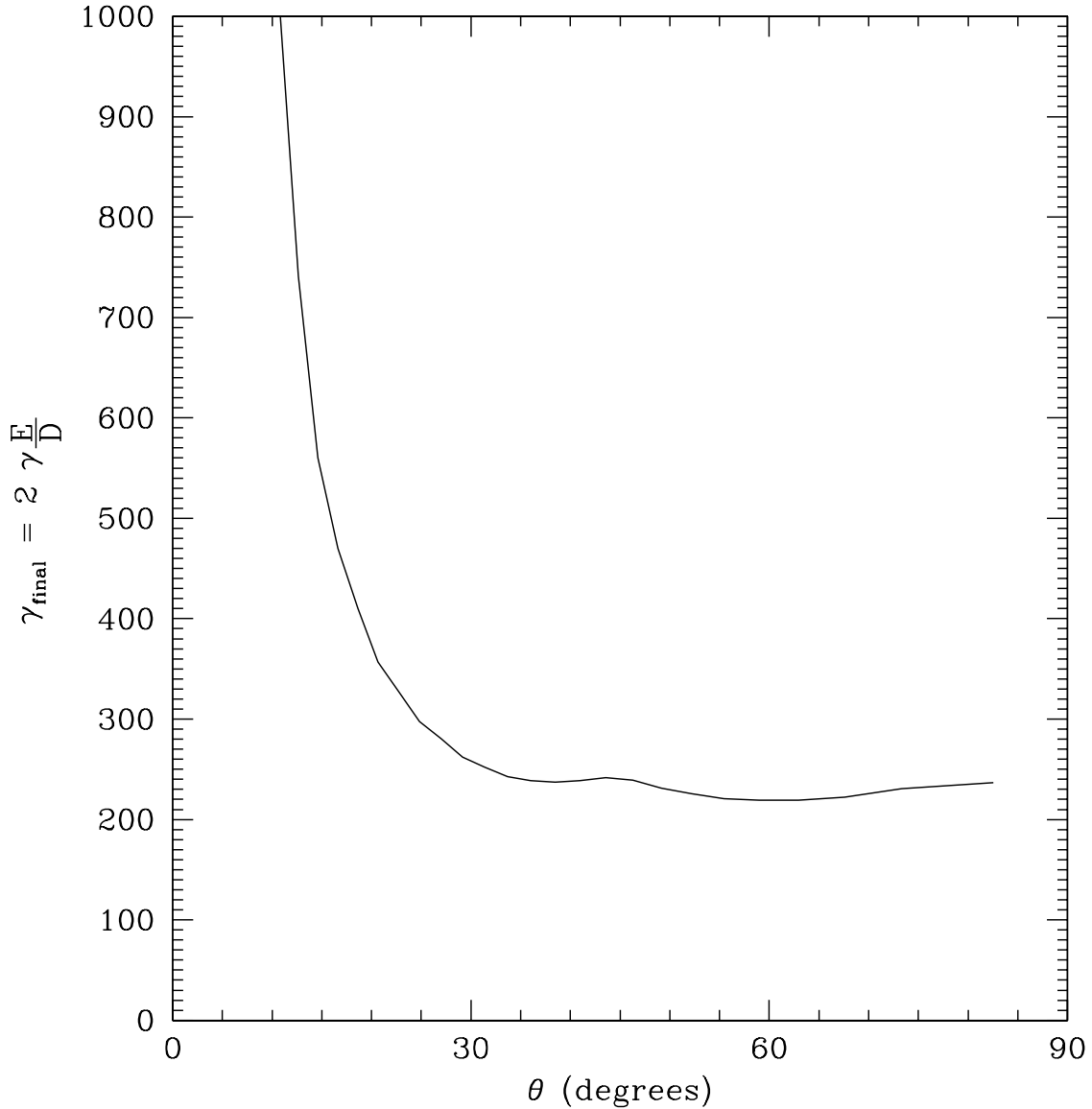


Fig. 3.— The terminal (final) Lorentz factor, $\gamma_{\text{final}} = 2\gamma E/D$, for $\gamma, E/D \gg 1$, from 3D simulations as a function of angle from the rotation axis of the binary system in the plane described by said axis and the line connecting the two stars. The local Lorentz factor is γ . Thus 0° is along the rotation axis and 90° corresponds to being directly behind one of the stars. The most energetic material, $\gamma_{\text{final}} \rightarrow \infty$, is located within a narrow region, $\theta < 15^\circ$, on the symmetry plane between the two stars.

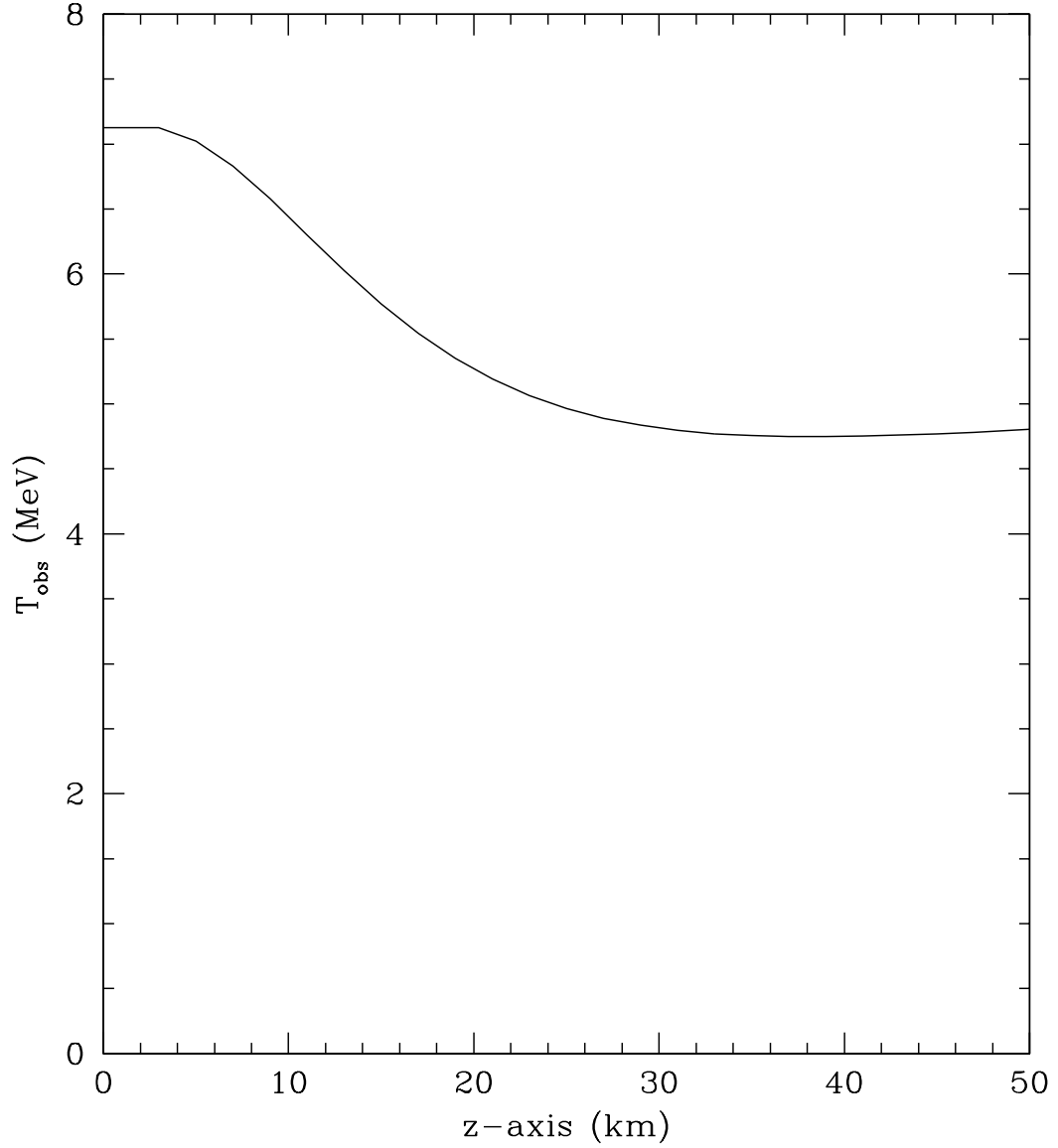


Fig. 4.— From the 3D code, the observed temperature at infinity, $T_{obs} \propto \alpha(W^3E)^{1/4}$ of the baryon-free pair plasma along the z -axis of rotation. Most of the plasma is at the high value of z hence this observed average effective temperature will be near 5 MeV.

5. Results

An example of a 3D run is shown in Fig. 1. An edit of the final Lorentz factor, γ_{final} , as a function of angle from the rotation axis in the plane defined by the rotation axis and the line connecting the two stars is shown in Fig. 3. One can see that the highest energy per baryon occur along the rotation axis. From this figure one gets the scale of the opening angle of this high energy material: $\sim 15^\circ$. The simulation does not sufficiently resolve the region of high E/D at low angles. Very little baryon mass will make it into this region of high energy density, thus we expect E/D to be effectively infinite on the rotation axis. Thus for viewers within this angle we have a thermal burst dominated by e^+e^- pair-photon plasma as described in (Salmonson et al. 2001). An edit of the observed temperature $T_{\text{obs}} \propto \alpha(W^3 E)^{1/4}$ is shown in Fig. 4, where we have used quantities defined in eqns. (3, 6, 9).

One can see from Fig. 3 that, depending on the observer angle with respect to the axis of rotation, a wide range of baryon loadings, parameterized by E/D , will be observed. Thus we study the range of expected observed signals as it depends on E/D . Herein we assume a correspondence between the ratio of energy to mass, \mathcal{E}/\mathcal{M} , of the spherically symmetric calculations of Section 3 to the ratio of energy to mass *coordinate densities*, E/D , as taken from the 3D code runs. As such, we expect a thermal burst for observers along the axis of rotation of the stars and within an angle $\sim 15^\circ$ where no baryons are deposited and thus $E/D \rightarrow \infty$. As seen in Fig. 3, for increasing θ from the rotation axis, E/D decreases rapidly to ~ 100 .

For all $E/D = \mathcal{E}/\mathcal{M} < 10^5$ all of the energy of the pair plasma is deposited into the baryons and therefore a prompt thermal burst does not occur. Instead, the mass, \mathcal{M} , of baryons moving with Lorentz factor, $\gamma_{\text{final}} = \mathcal{E}/\mathcal{M}$, sweep into the interstellar medium, thus forming a collisionless shock, and decelerate according to (e.g. Piran 2000)

$$\mathcal{E} = \gamma_{\text{final}}\mathcal{M} = 4\pi\rho\gamma^2r^3 \quad (13)$$

for

$$r > r_{\text{dec}} \equiv \left(\frac{\mathcal{E}}{4\pi\rho c^2\gamma_{\text{final}}^2} \right)^{1/3} \sim 10^{16}\gamma_{300}^{-2/3}E_{52}^{1/3}n_1^{-1/3} \text{ cm} \quad (14)$$

where r_{dec} is the deceleration radius, ρ is the interstellar medium (ISM) density, $n_1 \equiv \rho/m_p$ cm^{-3} is the ISM baryon number density, $\gamma_{300} \equiv \gamma/300$ and $E_{52} \equiv \mathcal{E}/(10^{52} \text{ ergs})$. This model was worked out in detail in Salmonson et al. (2001). The shock will emit synchrotron radiation as it decelerates with a characteristic luminosity $L \sim (n_1\gamma_{300}^8)^{1/3}E_{52}^{2/3}10^{51} \text{ ergs s}^{-1}$ at a characteristic photon energy $\epsilon \sim 200\sqrt{n_1}\gamma_{300}^4 \text{ keV}$ and a duration on the deceleration timescale $t_{\text{dec}} = r_{\text{dec}}/2\gamma^2c \sim 3(E_{52}/n_1/\gamma_{300}^8)^{1/3} \text{ s}$. Note that for $\gamma \lesssim 300$ this timescale is consistent with long bursts: $> 3 \text{ s}$.

A distinct feature of this progenitor model, since the wind comes from the surface of a neutron star, is that most of the baryons will be in the form of neutrons (say 90%). Thus these neutrons will not couple with the ISM magnetic field and will pass by the decelerating protons. These neutrons will decay back to protons on a timescale of a neutron half-life, $\tau_{n,1/2} \approx 1000$ s, which happens at a radius $R_{decay} = \gamma c \tau_{n,1/2} \sim \gamma_{300} 10^{16}$ cm. Comparing this radius with the deceleration radius, r_{dec} , we see that $r_{dec} > R_{decay}$ for $\gamma < 300$, i.e. the neutrons have decayed into protons before reaching the deceleration radius. So we expect this effect to be important for $\gamma = \mathcal{E}/\mathcal{M} > 300$ (Fig. 5).

Another characteristic Lorentz factor $\gamma = \mathcal{E}/\mathcal{M}$ is when the time, in the fluid frame, to reach the deceleration radius is shorter than the deposition time, $\Delta t = 0.1$ s. The fluid frame deposition distance is $\Delta r' = \gamma c \Delta t \sim \gamma_{300} 10^{12}$ cm. Also in the fluid frame, the deceleration distance is $r'_{dec} = r_{dec}/\gamma \sim 10^{15} (n_1 \gamma_{300}^5)^{-1/3}$ cm. These are equal at $\gamma \approx 1500$ (Fig. 5). Thus for $\gamma > 1500$ the plasma deposited at the beginning of the deposition time has begun to decelerate before the plasma has completed deposition, so the assumption that the plasma is a thin, shocked shell plowing into the ISM is invalid. Instead, energy will be continuously deposited into the shock.

An important caveat for these high Lorentz factors, $\gamma \gg 300$, is that they likely are beyond the regime of validity for the collisionless shock. The detailed physics behind such shocks is not well understood (e.g. Piran 2000) and assumes that the kinetic energy of the baryons, $(\gamma - 1)m_p c^2$, will effectively amplify the magnetic field and energize the electrons. However, low densities of ultra-high energy baryons will inefficiently couple with the ISM and thus the collisionless shock approximation will be invalid.

Again, for energy, $\mathcal{E} = 10^{52}$ ergs, with photon energy $\epsilon \approx 200 \gamma_{300}^4$ keV, the observed photon fluence seen at a distance, R , will be $\mathcal{E} \xi / 4\pi R^2 \epsilon \approx 250 \xi \gamma_{300}^{-4} R_{Gpc}^{-2}$ cm $^{-2}$, where $R_{Gpc} \equiv R/(1 \text{ Gigaparsec})$ and ξ is an efficiency factor which may be about 10%. For example, given $\gamma = 1500$, we expect a fluence of 0.04 photons cm $^{-2}$ with characteristic energy $\epsilon \approx 0.1$ GeV over a duration $t_{dec} \approx 0.04$ s. So such a burst would be far from recognizable as such (Fig. 5).

6. Discussion

A key result of the 3D numerical simulations (Fig. 3) is that the emission from this system is bimodal: about half of the total energy is deposited as a pure, baryon-free, $E/D \rightarrow \infty$, pair plasma along a ‘fan’ of angular half-width $\theta = 15^\circ$ along the symmetry plane between the neutron stars, and the other half of the total energy is blown off of the neutron stars as a wind with $E/D \approx 300$. Very little of the energy is deposited in intermediate regimes of

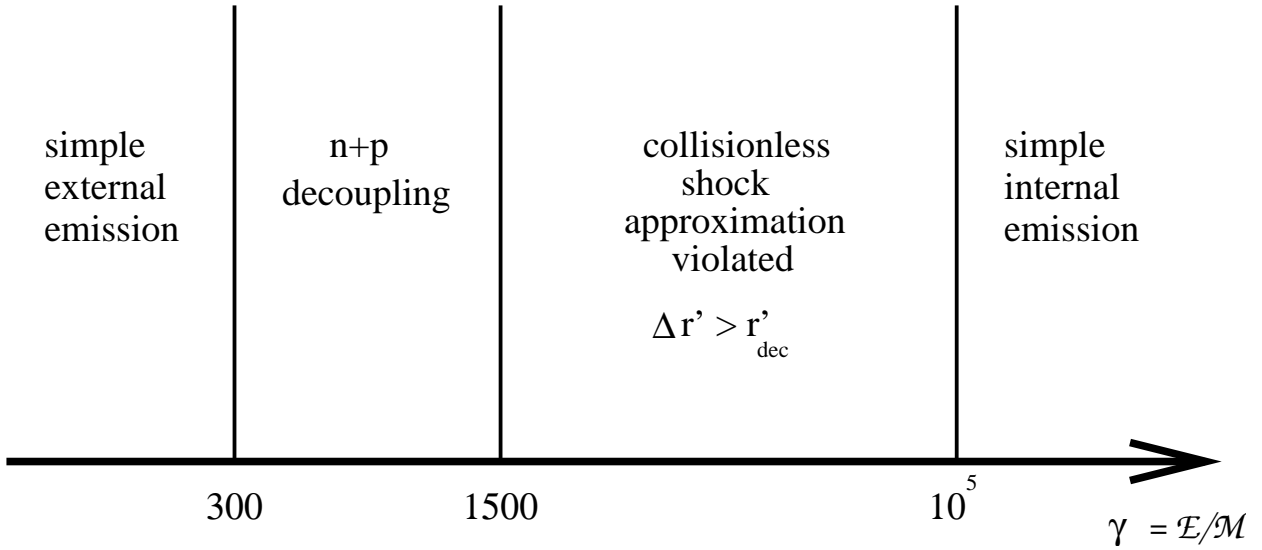


Fig. 5.— A schematic figure representing the physical regions along the spectrum of $\gamma = \mathcal{E}/\mathcal{M}$ discussed in Section 5. A simple external shock results for $\gamma < 300$. For $300 < \gamma < 1500$ the neutrons will be decoupled from the protons and thus will decay and shock at a larger radius, thus creating a smeared external shock. For $1500 < \gamma < 10^5$ the external shock cannot be considered a simple thin shock and the theory of collisionless shocks is likely violated. In the region $\gamma > 10^5$, the energy remains in the photons from the original pair plasma and thus a simple internal shock results as discussed in Section 3 and is detailed in Fig. (2).

E/D . As such we analyse the expected observations from this model.

The solid angle subtended by the fan of baryon-free plasma is $\Omega_{fan} = 4\pi \sin \theta$ and the wind blows off into the rest of space, $\Omega_{wind} = 4\pi(1 - \sin \theta)$. Therefore the fluence from each component at a distance R for total energy \mathcal{E} is

$$\begin{aligned} F_{fan} &= \frac{\xi \mathcal{E}/2}{\Omega_{fan} R^2} = \frac{\xi \mathcal{E}}{8\pi \sin \theta R^2} \\ F_{wind} &= \frac{\xi \mathcal{E}/2}{\Omega_{wind} R^2} = \frac{\xi \mathcal{E}}{8\pi(1 - \sin \theta) R^2} \end{aligned} \quad (15)$$

where ξ is an efficiency factor. Now the system is rotating so an observer with angle, ψ , from the rotation axis will see a mixture of the fan and wind, unless he is located within an angle $\psi < \theta$. Since the period of rotation of the system is much smaller than the energy deposition timescale, $\Delta t = 0.1$ s, we average over the fluences from the wind and the fan to get a total average fluence. The proportion of a rotation subtended by the fan is $2/\pi \arcsin(\theta/\sin \psi)$ for $\theta \lesssim \psi \leq \pi/2$ and is unity for $0 < \psi < \theta$. So the average fluence contributed by the fan as a function of viewing angle is (Fig. 6)

$$\overline{F}_{fan}(\psi) = \frac{\mathcal{E}}{8\pi R^2} \begin{cases} \frac{2/\pi \arcsin(\theta/\sin(\psi))}{\sin \theta} & \text{for } \theta \lesssim \psi \leq \pi/2, \\ \frac{1}{\sin \theta} & \text{for } 0 < \psi < \theta, \end{cases} \quad (16)$$

and that of the wind is

$$\overline{F}_{wind}(\psi) = \frac{\mathcal{E}}{8\pi R^2} \begin{cases} \frac{1-2/\pi \arcsin(\theta/\sin(\psi))}{1-\sin \theta} & \text{for } \theta \lesssim \psi \leq \pi/2, \\ 0 & \text{for } 0 < \psi < \theta. \end{cases} \quad (17)$$

The total average fluence is

$$\overline{F}(\psi) = \overline{F}_{fan}(\psi) + \overline{F}_{wind}(\psi). \quad (18)$$

An observer within $0 < \psi < \theta$ sees only the fan emission. This is effectively a jet of opening half-angle $\theta = 15^\circ$. Such an observer sees a jet of strong thermal emission over a timescale of 0.1 s. For $\theta = 15^\circ = \pi/12$ we have

$$\begin{aligned} \overline{F}(\psi = 0) &= 1.6 \times 10^{-4} \frac{\xi E_{52}}{R_{Gpc}^2} \text{ ergs cm}^{-2} \\ \overline{F}(\psi = \pi/2) &= 7.3 \times 10^{-5} \frac{\xi E_{52}}{R_{Gpc}^2} \text{ ergs cm}^{-2} \end{aligned} \quad (19)$$

so an observer along the jet ($\psi < \theta$) will see roughly twice the fluence in a short, 0.1 s, thermal, $T_{obs} \approx 5$ MeV, gamma-ray burst, than an off-axis observer ($\psi \sim \pi/2$) who will see a synchrotron burst of duration ~ 3 s with characteristic photon energy 200 keV.

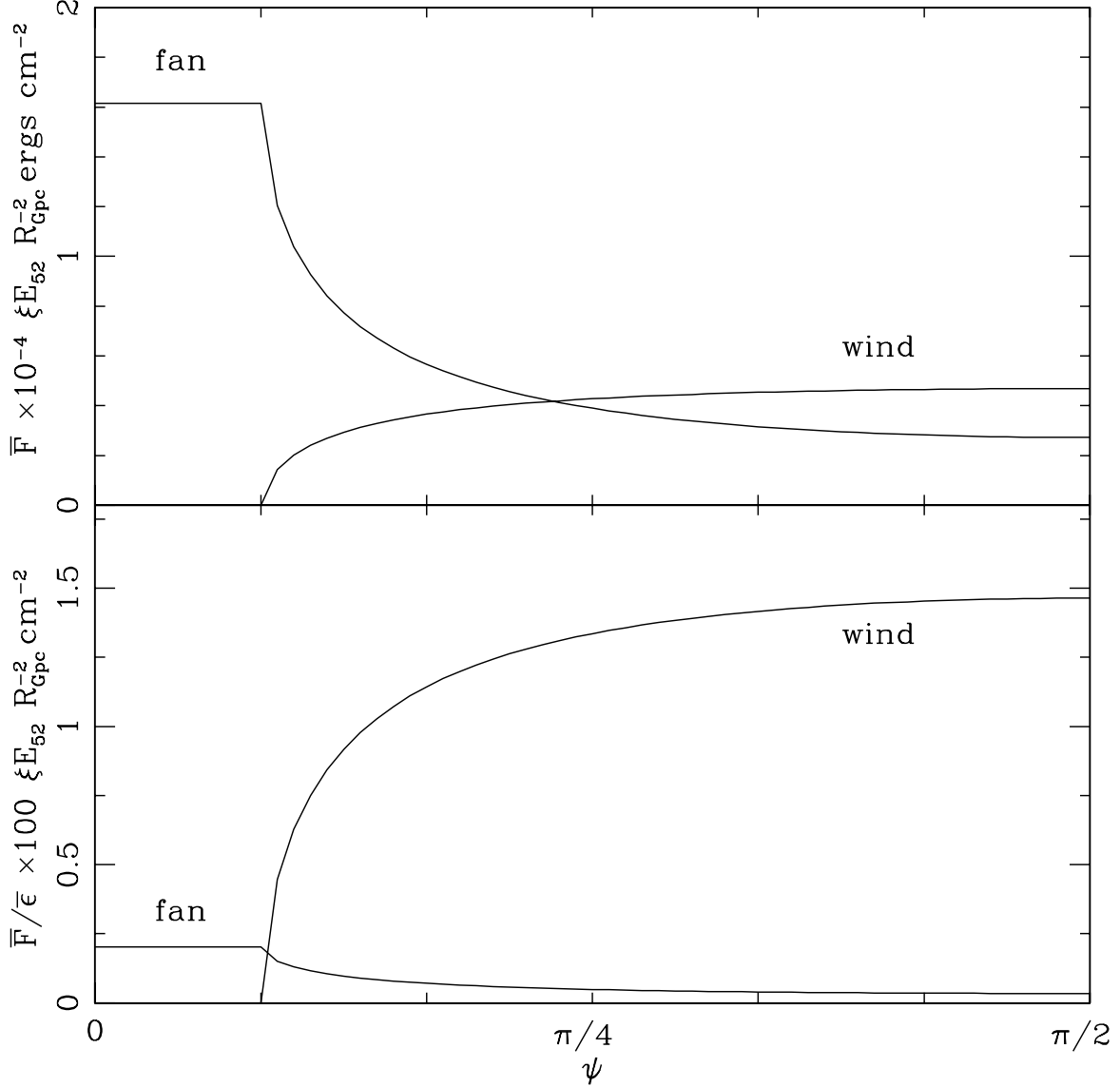


Fig. 6.— The top figure shows the average fluence \bar{F} of the fan (Eqn. 16) and the wind (Eqn. 17) as a function of viewing angle ψ . The bottom figure shows number fluence, \bar{F} divided by the characteristic photon energy for the fan, $\bar{\epsilon}_{fan} \approx 5$ MeV (Fig. 4), and the wind, $\bar{\epsilon}_{wind} \approx 200$ keV (Sec. 5). This demonstrates that most of the energy comes from the fan while most of the photons come from the wind. A viewer within $\psi < 15^\circ = \pi/12$ will see only the fan emission, which effectively constitutes a jet of half-opening angle 15° .

In conclusion, when the binary system is viewed within 15° of the axis of rotation, we have a model for short gamma-ray bursts, ~ 0.1 s, which have hard spectra, several MeV. In addition, when the binary system is viewed at angles larger than 15° from the rotation axis, our model yields a second group of bursts, 30 times more common, with soft spectra, a few hundred keV, and intermediate time duration of 1 to 5 s. The energy available depends on the neutron star equation of state and the masses of the neutron stars. The energy in a burst could range from 10^{50} ergs to a few times 10^{52} ergs. From Fig. 6 we see that if the detector is primarily sensitive to number counts then at intermediate viewing angles the fan contribution to the signal may be missed. The pure fan signal, i.e. a jet viewed within 15° of the rotation axis, will have no afterglow, but the fan plus wind would have an afterglow and a small contribution of high energy photons. Jensen et al. (2001) have observed a 2 s burst with an afterglow. Unfortunately the high energy detector data was not obtained.

This work was performed under the auspices of the U.S. Department of Energy by University of California Lawrence Livermore National Laboratory under contract W-7405-ENG-48.

REFERENCES

- Connaughton V. 2000, in AIP Conf. Proc. 526: Gamma-ray Bursts, 5th Huntsville Symposium, p. 385
- Derishev, E. V., Kocharovsky, V. V., Kocharovsky, V. V. 1999, ApJ, 521, 640
- Fuller G. M., Pruet J., Abazajian K. 2000, Phys. Rev. Lett., 85, 2673
- Gandolfi G. e. a. 2001, BeppoSAX Results on Short Gamma Ray Bursts, to appear in the proceedings of Gamma-Ray Burst and Afterglow Astronomy 2001
- Jensen B. L. et al. 2001, A&A, 370, 909
- Kouveliotou C., Meegan C. A., Fishman G. J., Bhat N. P., Briggs M. S., Koshut T. M., Paciesas W. S., Pendleton G. N. 1993, ApJ, 413, L101
- Lazzati D., Ramirez-Ruiz E., Ghisellini G. 2001, Possible detection of hard X-ray afterglows of short gamma-ray bursts, accepted to A&AL, astro-ph/0110215
- Mathews G. J., Wilson J. R. 1997, ApJ, 482, 929
- Mathews G. J., Wilson J. R. 2000, Phys. Rev. D, 61, 127304
- Norris J. P., Scargle J. D., Bonnell J. T. 2000, AAS/High Energy Astrophysics Division, 32, 3402
- Paciesas W. S., Preece R. D., Briggs M. S., Malozzi R. S. 2001, Spectral Properties of Short Gamma-Ray Bursts, astro-ph/0109053
- Piran T. 2000, Phys. Rep., 333, 529
- Ruffini R., Salmonson J. D., Wilson J. R., Xue S.-S. 2000, A&A, 359, 855
- Salmonson J. D., Wilson J. R. 1999, ApJ, 517, 859
- Salmonson J. D., Wilson J. R. 2001, ApJ, 561, 950
- Salmonson J. D., Wilson J. R., Mathews G. J. 2001, ApJ, 553, 471